Mathematical Biosciences and Engineering

http://www.aimspress.com/journal/mbe

MBE, 20(1): 1344–1375.
DOI: 10.3934/mbe.2023061
Received: 06 August 2022
Revised: 21 October 2022
Accepted: 21 October 2022
Published: 28 October 2022

Research article

Mathematical analysis of a COVID-19 model with different types of quarantine and isolation

Maryam Al-Yahyai[1], Fatma Al-Musalhi[2,*], Ibrahim Elmojtaba[1] and Nasser Al-Salti[3]

[1] Department of Mathematics, Sultan Qaboos University, Muscat, Oman
[2] Centre of Preparatory Studies, Sultan Qaboos University, Muscat, Oman
[3] Department of Applied Mathematics and Science, National University of Science and Technology, Muscat, Oman

* **Correspondence:** Email: fatma@squ.edu.om.

Abstract: A COVID-19 deterministic compartmental mathematical model with different types of quarantine and isolation is proposed to investigate their role in the disease transmission dynamics. The quarantine compartment is subdivided into short and long quarantine classes, and the isolation compartment is subdivided into tested and non-tested home-isolated individuals and institutionally isolated individuals. The proposed model has been fully analyzed. The analysis includes the positivity and boundedness of solutions, calculation of the control reproduction number and its relation to all transmission routes, existence and stability analysis of disease-free and endemic equilibrium points and bifurcation analysis. The model parameters have been estimated using a dataset for Oman. Using the fitted parameters, the estimated values of the control reproduction number and the contribution of all transmission routes to the reproduction number have been calculated. Sensitivity analysis of the control reproduction number to model parameters has also been performed. Finally, numerical simulations to demonstrate the effect of some model parameters related to the different types of quarantine and isolation on the disease transmission dynamics have been carried out, and the results have been demonstrated graphically.

Keywords: COVID-19; quarantine; isolation; reproduction number; stability analysis; bifurcation analysis; sensitivity analysis

1. Introduction

The COVID-19 pandemic first initiated in December 2019 in the city of Wuhan, China [1], and since then, it has been spreading worldwide. The coronavirus disease 19 is caused by severe acute respiratory syndrome coronavirus 2 (SARS- CoV-2) [2, 3]. On February 24, 2020, the Oman Ministry Of Health

registered the first two COVID-19 cases for Omani women associated with travel. On January 30, 2020, the World Health Organization (WHO) declared the outbreak a public health emergency of international concern [4]. On March 11, 2020, it characterized the outbreak as a pandemic [5].

Governments around the world regularly respond to the announcements made by the WHO, and different medical protocols are followed depending on the epidemiological status. On the same day of declaring COVID-19 as a pandemic, the Omani government responded and His Majesty The Sultan issued his royal orders to set up a supreme committee for dealing with the developments resulting from the spread of COVID-19 [6]. Since then, the Supreme Committee has made many decisions and regulations to help monitor and protect the country's healthcare system. As is the case in many countries, the main methods adopted for controlling the spread of COVID-19 have been a lockdown, quarantine, isolation and creating awareness among individuals to adopt social distancing and maintain personal hygiene. By the end of December 2020, some types of vaccines against COVID-19 had been approved and distributed [7]. However, authorities still recommend that people practice non-pharmaceutical intervention strategies (such as social distancing and wearing masks) to avoid and fight against the spread of COVID-19. The timeline chart in Figure 1 summarizes the events mentioned above.

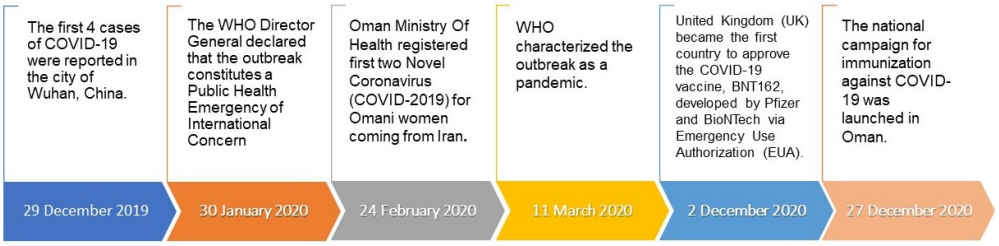

Figure 1. COVID-19 timeline.

Many researchers proposed mathematical models to study the effectiveness of the various strategies and interventions in controlling the spread of COVID-19 before any effective vaccine had been developed. Aronna, Guglielmi and Moschen [8] proposed a compartmental model for the dynamics of COVID-19. They took into account the presence of asymptomatic infections, and also the main policies that had been adopted by several countries to fight the disease, these being: isolation, quarantine and testing. They modeled isolation by separating the population into two groups: one composed of essential workers that keep working during the pandemic, and the other group consisting of people that were recommended to stay at home. They showed that people that remain in isolation significantly reduce their probability of contagion, so risk groups should be recommended to maintain a low contact rate during the course of the epidemic.

Džiugys et al. [9] developed a model under quarantine conditions and methods to estimate quarantine effectiveness. It is based on the daily growth rate of new infections. Using collected epidemiological data of the COVID-19 pandemic, they found that the daily growth rate of new infections has a tendency to decrease linearly when the quarantine is imposed until it reaches a constant value.

Varghese et al. [10] formulated a deterministic compartmental model including various stages of

infection to study the spreading of COVID-19; they estimated the model parameters by fitting the model with the reported data in Oman. They proved the model's steady state, stability, and final pandemic size mathematically. In addition, they performed a sensitivity analysis to identify the key model parameters and found that contact with symptomatic moderately infected is more significant in spreading the disease.

For more compartmental models based on ordinary differential equations we refer the reader to [11–17]. For example, the authors of [11] developed a mathematical model to investigate the role of the diagnosis rate in the transmission dynamics of COVID-19 together with the combined effects of quarantine and isolation. They concluded that quarantine and diagnosis, especially for the presymptomatic humans, play the most crucial role in controlling the disease transmission.

The researchers in [18] found that if isolation can be implemented effectively (high efficacy and coverage), then the quarantine of people suspected of contracting COVID-19 may not be necessary. Many studies with mathematical models based on fractional differential equations also investigated COVID-19 transmission dynamics. Oud et al. [19] considered a fractional model to explore the transmission dynamics and possible control of the COVID-19 pandemic in Pakistan. Initially, they examined a model without optimal control variables. It provided a good fit to the reported cases and then estimated the model parameters using the non-linear least square curving fitting approach. They further reformulated the model by adding two time-dependent control variables. They observed that the most effective strategy to minimize the disease is the implementation of maintaining strict social distancing and contact tracing to quarantine the exposed people. Other studies can be found in References [20–23]. The researches in [24] found that fractional models better predict future dynamics and give closer estimates to the real data than integer-order models.

In this paper, we propose and analyze a mathematical model to study the roles of different types of quarantine and isolation in COVID-19 transmission dynamics. In particular, we will consider short- and long-term quarantines and home and institutional isolations, taking Oman as a case study and utilizing its COVID-19 data for model parameter estimations. Although the literature is rich in compartmental models, and the effects of quarantine and isolation on COVID-19 spread are well established, our model attempts to reflect the situation during the period of time when data were collected for fitting. The model aims to investigate the roles of different types of quarantine and isolation on the dynamics of COVID-19. Hence our main contribution is the inclusion of corresponding classes of quarantine and isolation to capture the effects of the related control strategies that were implemented by Oman's health authorities on disease dynamics.

The paper is organized as follows. The model formulation is described in Section 2. The model analysis includes the positivity, boundedness of the solution, control reproduction number and existence and stability analysis of disease-free and endemic equilibrium points, which are discussed in Sections 3 and 4. Furthermore, bifurcation analysis and sensitivity analysis are also presented. The fitting of the model parameters and numerical analysis of the model using estimated parameters are given in Section 5 to illustrate the effects of quarantine and isolation on the spread of the disease. Finally, the conclusion is given in Section 6.

2. Model formulation

The formulation of this model is based on classifying the human population $N(t)$ according to their health status into 11 classes. These classes are susceptible $S(t)$, exposed $E(t)$, asymptomatic $A(t)$, presymptomatic $P(t)$, symptomatic $I(t)$, quarantined for a short time (at home or institutionally) $Q_S(t)$, quarantined for a long time (mostly at home) $Q_L(t)$, non-tested home-isolated $J_N(t)$, tested home isolated $J_H(t)$, tested isolated at health institutions $J_I(t)$ and recovered $R(t)$, thus,

$$N = S + E + A + P + I + Q_S + Q_L + J_N + J_H + J_I + R$$

2.1. Model assumptions and description

Susceptible individuals, $S(t)$, are those at risk of becoming infected. They are recruited into the population at a constant rate Λ. They acquire COVID-19 by direct contact with asymptomatic, presymptomatic, symptomatic, non-tested and tested home-isolated at rates of β_A, β_P, β_I, β_N and β_H, respectively. It is assumed that there is no transmission from the institutional isolation class. This class is assumed to be completely isolated from the susceptible group.

Following governmental regulations regarding travel restrictions, it is assumed that some susceptible individuals undergo a short quarantine, $Q_S(t)$, at a rate of ρ_S and leave the class by either natural death, returning back to the susceptible class at a rate of λ_S after 14 days or by moving to long quarantine, $Q_L(t)$, at a rate of α_S. Long quarantine is considered a behavioural practice adhered to by some people due to their awareness or fear. Individuals in the long quarantine class leave by natural death or return back to the susceptible class at a rate of λ_L.

All newly infected individuals enter the exposed class $E(t)$, in which they remain non-infectious during their latent period. After this period, they become infectious at different rates λ_A, λ_P or λ_I as asymptomatic, presymptomatic or symptomatic, respectively.

Asymptomatic individuals, $A(t)$, are infected and contagious but do not show any symptoms until they recover. It is assumed that they leave their class by a natural death, isolation at home for non-tested individuals at a rate of ρ_A, getting diagnosed and isolated at home (health institutions) at a rate of $\varepsilon_A(\theta_A)$ or recovery at a rate of γ_A.

Presymptomatic infectees, $P(t)$, currently have no symptoms but will develop symptoms after some time. It is assumed that they leave their class due to natural death, tested positive and hence are isolated at homes/health institutions at a rate of ε_P/θ_P or move to the infected class with symptoms at a rate of σ_P when symptoms are onset. As a result of contact-tracing or human behaviour, some presymptomatic individuals move to the non-tested home isolated class at a rate of ρ_P. It is assumed that there is no disease-related death in the presymptomatic class.

Individuals in the symptomatic class, $I(t)$, are those with mild COVID-19 symptoms but have not been tested. It is assumed that when diagnosed or symptoms become severe, medical care is needed; some are moved to tested home isolation at a rate of θ_I, and some are moved to institutional isolation at a rate of ε_I, while the remaining stay in the symptomatic class until they recover at a rate of γ_I. No disease-related death is assumed in this class, but natural death may occur.

Non-tested home-isolated individuals, $J_N(t)$, are those individuals with suspected infection, with or without symptoms, who have not been tested. They come from the exposed class at a rate of ρ_E, from the asymptomatic class at a rate of ρ_A and from the presymptomatic class at a rate of ρ_P. It is assumed

that some people have COVID-19 symptoms but do not wish to obtain a diagnosis. Instead, they prefer to isolate themselves in their home. Also, due to identification by contact tracing, some are instructed to isolate themselves at home, and they are usually tracked by electronic track-bands to make sure that they adhere to isolation. Another group tends to self-isolate themselves at home as human behaviour. All of these categories are classified in the $J_N(t)$ compartment.

Depending on their symptoms or random testing, it is assumed that non-tested home isolated individuals leave their class by transferring to tested home (institutional) isolation at a rate of $\varepsilon_N(\theta_N)$. Some leave the class after recovery at a rate of γ_N or due to natural death.

The tested home-isolated infectees ($J_H(t)$) leave their class by natural death, disease-related death at a rate of δ_H, moving to institutional isolation at a rate of θ_H for health care after their symptoms become more severe or recovery at a rate of γ_H.

It is assumed that individuals isolated at health institutions, $J_I(t)$, leave this class due to natural death, recovery at a rate of γ_D, disease-related death at a rate of δ_D or moving to home isolation at a rate of ε_D after they have received the required health care. The above description is summarized in the flow chart in Figure 2.

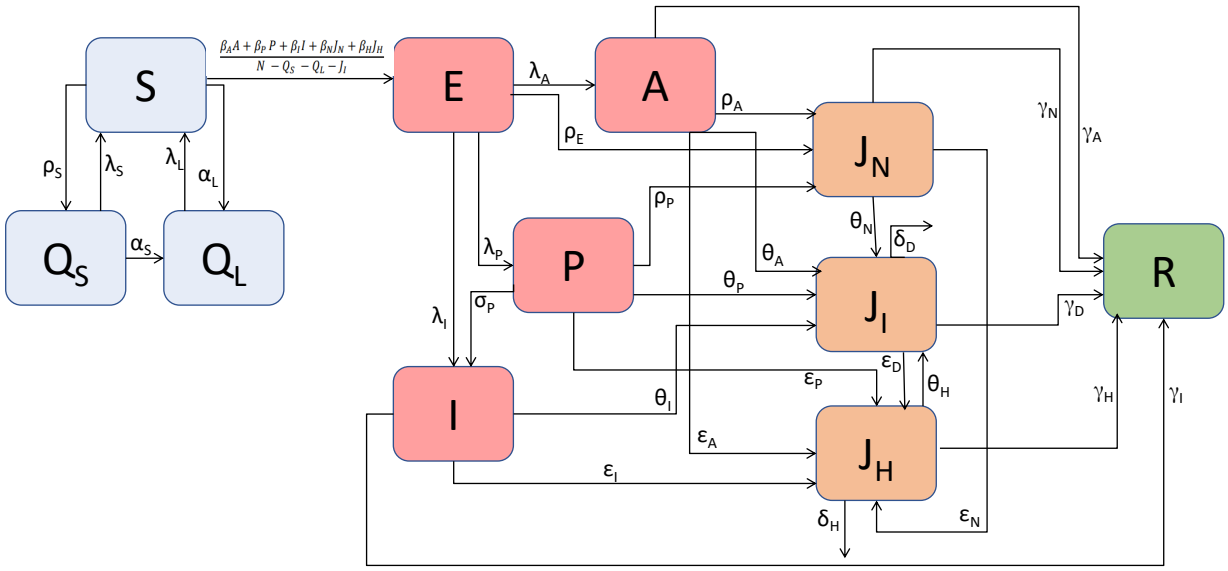

Figure 2. Flow diagram of the model (2.1) .

2.2. *Model equations*

Based on the above description, the proposed mathematical model is given by the following set of differential equations:

$$\frac{dS}{dt} = \Lambda - \frac{(\beta_A A + \beta_P P + \beta_I I + \beta_H J_H + \beta_N J_N)\, S}{N - Q_S - Q_L - J_I} - (\mu + \alpha_L + \rho_S)S + \lambda_S Q_S + \lambda_L Q_L$$

Table 1. Definition of the state variables in the model (2.1).

State variable	Class description	State variable	Class description
$S(t)$	Susceptible	$Q_L(t)$	Long quarantined
$E(t)$	Exposed, but not infectious	$J_N(t)$	Non-tested home isolated
$A(t)$	Asymptomatic	$J_H(t)$	Tested home-isolated
$P(t)$	Presymptomatic	$J_I(t)$	Tested isolated at health institutions
$I(t)$	Symptomatic	$R(t)$	Recovered
$Q_S(t)$	Short quarantined	$N(t)$	Total population

$$
\begin{aligned}
\frac{dE}{dt} &= \frac{(\beta_A A + \beta_P P + \beta_I I + \beta_H J_H + \beta_N J_N)\, S}{N - Q_S - Q_L - J_I} - (\mu + \lambda_A + \lambda_P + \lambda_I + \rho_E)E \\
\frac{dA}{dt} &= \lambda_A E - (\mu + \varepsilon_A + \theta_A + \gamma_A + \rho_A)A \\
\frac{dP}{dt} &= \lambda_P E - (\mu + \varepsilon_P + \sigma_P + \theta_P + \rho_P)P \\
\frac{dI}{dt} &= \lambda_I E + \sigma_P P - (\mu + \varepsilon_I + \gamma_I + \theta_I)I \\
\frac{dQ_S}{dt} &= \rho_S S - (\mu + \lambda_S + \alpha_S)Q_S \\
\frac{dQ_L}{dt} &= \alpha_L S + \alpha_S Q_S - (\mu + \lambda_L)Q_L \\
\frac{dJ_N}{dt} &= \rho_E E + \rho_A A + \rho_P P - (\mu + \gamma_N + \varepsilon_N + \theta_N)J_N \\
\frac{dJ_H}{dt} &= \varepsilon_A A + \varepsilon_P P + \varepsilon_I I + \varepsilon_N J_N + \varepsilon_D J_I - (\mu + \delta_H + \gamma_H + \theta_H)J_H \\
\frac{dJ_I}{dt} &= \theta_A A + \theta_P P + \theta_I I + \theta_N J_N + \theta_H J_H - (\mu + \delta_D + \gamma_D + \varepsilon_D)J_I \\
\frac{dR}{dt} &= \gamma_A A + \gamma_I I + \gamma_H J_H + \gamma_D J_I + \gamma_N J_N - \mu R
\end{aligned}
\tag{2.1}
$$

where, $N'(t) = \Lambda - \delta_H J_H(t) - \delta_D J_I(t) - \mu N(t)$. Model state variables are defined in Table 1, and the parameters are defined in Table 2. For simplicity of the calculations, we denote the following:

$$
\begin{aligned}
&\eta = \mu + \alpha_L + \rho_S, && && \xi = \mu + \lambda_S + \alpha_S, \\
&a = \mu + \lambda_A + \lambda_P + \lambda_I + \rho_E, && b = \mu + \varepsilon_A + \theta_A + \gamma_A + \rho_A, && c = \mu + \varepsilon_P + \sigma_P + \theta_P + \rho_P, \\
&d = \mu + \varepsilon_I + \gamma_I + \theta_I, && e = \mu + \gamma_N + \varepsilon_N + \theta_N, && f = \mu + \delta_H + \gamma_H + \theta_H, \\
&g = \mu + \delta_D + \gamma_D + \varepsilon_D, && && h = (\mu + \lambda_L).
\end{aligned}
$$

Table 2. Parameters used in the model (2.1).

Parameter	Description
Λ	Recruitment rate.
μ	Natural death rate of humans
β_A	Transmission rate from asymptomatic.
β_P	Transmission rate from presymptomatic.
β_I	Transmission rate from symptomatic.
β_N	Transmission rate from non-tested home isolated.
β_H	Transmission rate from tested home-isolated.
λ_S	Moving rate from short quarantine to susceptible class.
λ_L	Moving rate from long quarantine to susceptible class.
λ_A	Rate at which exposed become asymptomatic.
λ_P	Rate at which exposed become presymptomatic.
λ_I	Rate at which exposed become infected with symptoms.
σ_P	Rate at which presymptomatic develop symptoms.
ε_A	Tested home isolation rate of asymptomatic
ε_P	Tested home isolation rate of presymptomatic
ε_I	Tested home isolation rate of symptomatic.
ε_N	Diagnosed rate of non-tested home isolated.
ε_D	Moving rate from institutional to home isolation.
α_L	Rate at which susceptible enters long quarantine.
α_S	Rate of movement from short to long quarantine.
γ_A	Recovery rate of asymptomatic
γ_I	Recovery rate of symptomatic.
γ_D	Recovery rate of diagnosed institutionally isolated.
γ_H	Recovery rate of diagnosed home isolated.
γ_N	Recovery rate of non-tested home-isolated.
δ_H	COVID-19 related death rate of tested home isolated.
δ_D	COVID-19 related death rate of institutionally isolated.
ρ_S	Rate at which susceptible enter short quarantine.
ρ_E	Rate at which exposed enters non-tested home isolation.
ρ_A	Rate at which asymptomatic enters non-tested home isolation.
ρ_P	Rate at which presymptomatic enter non-tested home isolation.
θ_A	Rate of institutional isolation of asymptomatic.
θ_P	Rate of institutional isolation of presymptomatic.
θ_I	Rate of institutional isolation of symptomatic.
θ_N	Rate of institutional isolation of non-tested home-isolated.
θ_H	Rate of institutional isolation of tested home-isolated.

3. Positivity and boundedness

In this section, we study the positivity and boundedness of solutions of the system (2.1) subject to the positive initial conditions

$$\mathbf{U}(0) > 0 \tag{3.1}$$

where

$$\mathbf{U} = (S, E, A, P, I, Q_S, Q_L, J_N, J_H, J_I, R)^T.$$

Theorem 1. Solutions of the model (2.1) with the initial conditions (3.1) are positive for all $t \geq 0$.

Proof Consider the first equation of the model (2.1):

$$\frac{dS}{dt} = \Lambda - \frac{(\beta_A A + \beta_P P + \beta_I I + \beta_H J_H + \beta_N J_N) S}{N - Q_S - Q_L - J_I} - \eta S + \lambda_S Q_S + \lambda_L Q_L,$$

and rewrite the force of the infection term in the form

$$\frac{(\beta_A A + \beta_P P + \beta_I I + \beta_H J_H + \beta_N J_N) S}{N - Q_S - Q_L - J_I} = \beta S.$$

Then

$$\frac{dS}{dt} = \Lambda - (\beta + \eta) S + \lambda_S Q_S + \lambda_L Q_L.$$

Let $t_1 = \sup(t > 0 \mid \mathbf{U}(t) > 0)$. We have

$$\frac{dS}{dt} + (\beta + \eta) S = \Lambda + \lambda_S Q_S + \lambda_L Q_L, \text{ with the integrating factor } e^{\int_0^t \beta(v)dv + \eta t}.$$

$$\text{Therefore, } \frac{d}{dt}\left[e^{\int_0^t \beta(v)dv + \eta t} S\right] = e^{\int_0^t \beta(v)dv + \eta t} \left[\Lambda + \lambda_S Q_S + \lambda_L Q_L\right].$$

Integrating both sides over $(0, t_1)$ gives

$$S(t_1) e^{\int_0^{t_1} \beta(v)dv + \eta t_1} - S(0) = \int_0^{t_1} [\Lambda + \lambda_S Q_S + \lambda_L Q_L] . e^{\int_0^t \beta(v)dv + \eta t} dt$$

$$S(t_1) = \left[S(0) + \int_0^{t_1} [\Lambda + \lambda_S Q_S + \lambda_L Q_L] . e^{\int_0^t \beta(v)dv + \eta t} dt\right] e^{-\int_0^{t_1} \beta(v)dv + \eta t_1} > 0.$$

Similarly, one can prove that the remaining components are positive at $t = t_1$. Hence, t_1 cannot be a supremum. Therefore, all solutions remain positive for all time $t \geq 0$.

Theorem 2. *All solutions $S(t)$, $E(t)$, $A(t)$, $P(t)$, $I(t)$, $Q_S(t)$, $Q_L(t)$, $J_N(t)$, $J_H(t)$, $J_I(t)$ and $R(t)$ of the model (2.1) with the given initial conditions (3.1) are bounded.*

Proof From Theorem 1, solutions of the model (2.1) with the positive initial conditions are positive for $t \geq 0$.

We have that $N = S + E + A + P + I + Q_S + Q_L + J_N + J_H + J_I + R$.

Thus, $\dfrac{dN}{dt} = \Lambda - \delta_H J_H(t) - \delta_D J_I(t) - \mu N(t) \leq \Lambda - \mu N(t)$.

Therefore, $\lim\limits_{t\to\infty} \sup N(t) \leq \dfrac{\Lambda}{\mu}$, and hence the solutions are bounded. The feasible invariant region is given by

$$\Omega = \left\{(S(t), E(t), A(t), P(t), I(t), Q_S(t), Q_L(t), J_N(t), J_H(t), J_I(t), R(t)) \in \mathbb{R}_+^{11} : N(t) \leq \frac{\Lambda}{\mu}\right\}.$$

4. Disease free equilibrium and control reproduction number

The disease free equilibrium (DFE) of the model is given by

$$E_0 = (S^*, 0, 0, 0, 0, Q_S{}^*, Q_L{}^*, 0, 0, 0, 0),$$

where

$$S^* = \frac{\Lambda\xi\, h}{\eta\,\xi\, h - \lambda_S\,\rho_S\, h - \alpha_L\,\lambda_L\,\xi - \lambda_L\,\alpha_S\,\rho_S},$$

$$Q_S{}^* = \frac{\Lambda\,\rho_S\, h}{\eta\,\xi\, h - \lambda_S\,\rho_S\, h - \alpha_L\,\lambda_L\,\xi - \lambda_L\,\alpha_S\,\rho_S},$$

$$Q_L{}^* = \frac{(\alpha_L\,\xi + \alpha_S\,\rho_S)\,\Lambda}{\eta\,\xi\, h - \lambda_S\,\rho_S\, h - \alpha_L\,\lambda_L\,\xi - \lambda_L\,\alpha_S\,\rho_S}.$$

Hence

$$E_0 = \left(S^*,\ 0,\ 0,\ 0,\ 0,\ \frac{\rho_S}{\xi}S^*,\ \frac{\alpha_L\,\xi + \alpha_S\,\rho_S}{h\,\xi}S^*,\ 0,\ 0,\ 0,\ 0\right).$$

The control reproduction number, denoted by R_c, is the number of secondary infections caused by a single infective in a totally susceptible population with control measures in place. It is calculated by using the next generation matrix (NGM) method [25] as follows. First, the matrix of new infection is

found to be

$$\mathcal{F} = \begin{bmatrix} \dfrac{(\beta_A A + \beta_P P + \beta_I I + \beta_N J_N + \beta_H J_H)\, S}{X} \\ 0 \\ 0 \\ 0 \\ 0 \\ 0 \\ 0 \end{bmatrix}, \tag{4.1}$$

where, $X = N - Q_S - Q_L - J_I$, and it has a Jacobian, evaluated at the DFE E_0 and $N^* = S^* + {Q_S}^* + {Q_L}^*$ that is given by

$$F = \begin{bmatrix} 0 & \beta_A & \beta_P & \beta_I & \beta_N & \beta_H & 0 \\ 0 & 0 & 0 & 0 & 0 & 0 & 0 \\ 0 & 0 & 0 & 0 & 0 & 0 & 0 \\ 0 & 0 & 0 & 0 & 0 & 0 & 0 \\ 0 & 0 & 0 & 0 & 0 & 0 & 0 \\ 0 & 0 & 0 & 0 & 0 & 0 & 0 \\ 0 & 0 & 0 & 0 & 0 & 0 & 0 \end{bmatrix}. \tag{4.2}$$

Then, the matrix of transition is given by

$$\mathcal{V} = \begin{bmatrix} aE \\ -\lambda_A E + bA \\ -\lambda_P E + cP \\ -\lambda_I E - \sigma_P P + dI \\ -\rho_E E - \rho_A A - \rho_P P + eJ_N \\ -\varepsilon_A A - \varepsilon_P P - \varepsilon_I I - \varepsilon_N J_N - \varepsilon_D J_I + fJ_H \\ -\theta_A A - \theta_P P - \theta_I I - \theta_N J_N - \theta_H J_H + gJ_I \end{bmatrix}, \tag{4.3}$$

and its Jacobian is

$$V = \begin{bmatrix} a & 0 & 0 & 0 & 0 & 0 & 0 \\ -\lambda_A & b & 0 & 0 & 0 & 0 & 0 \\ -\lambda_P & 0 & c & 0 & 0 & 0 & 0 \\ -\lambda_I & 0 & -\sigma_P & d & 0 & 0 & 0 \\ -\rho_E & -\rho_A & -\rho_P & 0 & e & 0 & 0 \\ 0 & -\varepsilon_A & -\varepsilon_P & -\varepsilon_I & -\varepsilon_N & f & -\varepsilon_D \\ 0 & -\theta_A & -\theta_P & -\theta_I & -\theta_N & -\theta_H & g \end{bmatrix}, \tag{4.4}$$

where a, b, c, d, e and f are as defined earlier after the model equations.

Now, NGM is given by

$$FV^{-1} = \begin{bmatrix} R_c & a_{12} & a_{13} & \dfrac{\beta_I}{d} + \dfrac{\beta_H(\varepsilon_I\, g + \varepsilon_D\, \theta_I\, H)}{d\, m} & \dfrac{\beta_N}{e} + \dfrac{\beta_H\,(\varepsilon_N\, g + \varepsilon_D\, \theta_N)}{e\, m} & \dfrac{\beta_H\, g}{m} & \dfrac{\beta_H\, \varepsilon_D}{m} \\ 0 & 0 & 0 & 0 & 0 & 0 & 0 \\ 0 & 0 & 0 & 0 & 0 & 0 & 0 \\ 0 & 0 & 0 & 0 & 0 & 0 & 0 \\ 0 & 0 & 0 & 0 & 0 & 0 & 0 \\ 0 & 0 & 0 & 0 & 0 & 0 & 0 \\ 0 & 0 & 0 & 0 & 0 & 0 & 0 \end{bmatrix},$$

where

$$\begin{aligned} a_{12} &= \frac{\beta_A}{b} + \frac{\beta_N \rho_A}{b\, e} + \frac{\beta_H\,(\varepsilon_A e g + \varepsilon_N \rho_A g + \varepsilon_D \theta_A e + \varepsilon_D \theta_N \rho_A)}{b\, e\, m}, \\ a_{13} &= \frac{\beta_P}{c} + \frac{\beta_I \sigma_P}{c\, d} + \frac{\beta_N \rho_P}{c\, e} + \frac{\beta_H\,(\varepsilon_P d e g + \varepsilon_I \sigma_P e g + \varepsilon_N \rho_P d g + \varepsilon_D \theta_P d e + \varepsilon_D \theta_I \sigma_P e + \varepsilon_D \theta_N \rho_P d)}{c\, d\, e\, m}, \\ m &= (g f - \theta_H \varepsilon_D)\,. \end{aligned}$$

The control reproduction number is the spectral radius of the NGM, i.e., $R_c = \rho(FV^{-1})$ and it is given by

$$R_c = R_A + R_P + R_I + R_N + R_H,$$

where

$$\begin{aligned} R_A &= \frac{\beta_A \lambda_A}{a\, b}, \qquad R_P = \frac{\beta_P \lambda_P}{a\, c}, \qquad R_I = \frac{\beta_I\,(c\lambda_I + \sigma_P \lambda_P)}{a\, c\, d}, \\ R_N &= \frac{\beta_N\,(\rho_E b c + \rho_A \lambda_A c + \rho_P \lambda_P b)}{a\, b\, c\, e}, \\ R_H &= \frac{\beta_H}{am}\left[g\left(\frac{\varepsilon_A \lambda_A}{b} + \frac{\varepsilon_P \lambda_P}{c} + \frac{\varepsilon_I\,(c\lambda_I + \sigma_P \lambda_P)}{c\, d} + \frac{\varepsilon_N\,(\rho_E b c + \rho_A \lambda_A c + \rho_P \lambda_P b)}{b\, c\, e} \right) \right] \end{aligned}$$

$$+\frac{\beta_H}{a\,m}\left[\varepsilon_D\left(\frac{\theta_A\lambda_A}{b}+\frac{\theta_P\lambda_P}{c}+\frac{\theta_I\,(c\lambda_I+\sigma_P\lambda_P)}{c\,d}+\frac{\theta_N\,(\rho_E bc+\rho_A\lambda_A c+\rho_P\lambda_P b)}{b\,c\,e}\right)\right].$$

Here, R_A, R_P, R_I, R_N, and R_H represent the contribution from asymptomatic, presymptomatic, symptomatic, non-tested home isolated and tested home isolated individuals, respectively.

Note that the reproductive number (R_c) is independent of short and long quarantines parameters. In fact, according to the assumptions in formulating the model, short and long quarantines have no direct impact on the control reproductive number (R_c). However, they play an essential and considerable role in separating susceptible humans from infected individuals and reducing the contact rate between them. Hence both types of quarantines contribute indirectly to controlling the spread of COVID-19.

4.1. Stability analysis of the disease free equilibrium

Studying the local stability of the DFE using linearization is complicated since the characteristic equation is of order 11. Therefore, global stability is checked instead by using the Lyapunov function method as described in [26].

Set

$$f(x,y) := (F-V)x - \mathcal{F}(x,y) + \mathcal{V}(x,y), \tag{4.5}$$

where $\mathcal{F}$, F, $\mathcal{V}$, and V as previously defined in (4.1), (4.2), (4.3) and (4.4), respectively, $x^T = [E \quad A \quad P \quad I \quad J_N \quad J_H \quad J_I] \in \mathbb{R}^7_+$ is the disease compartment, and $y^T = [S \quad Q_S \quad Q_L \quad R] \in \mathbb{R}^4_+$ is the non-disease compartment.

Then, the disease compartment can be written as $x' = (F-V)x - f(x,y)$ with $f(0,y) = 0$.

Let $w^T \geq 0$ be the left eigenvector of the non-negative matrix $V^{-1}F$ corresponding to the eigenvalue R_c. The vector is found to be $w^T = [0 \quad w_A \quad w_P \quad w_I \quad w_N \quad w_H \quad 0]$, where all of the entries are non-negative.

The following theorem provides a general method to construct a Lyapunov function for the system (2.1).

Theorem 4.1. *[26] Let F, V and $f(x,y)$ be as defined above. If $f(x,y) \geq 0$ in $\Omega \subset \mathbb{R}^{11}_+$, $F \geq 0$, $V^{-1} \geq 0$ and $R_c \leq 1$, then the function $Q = w^T V^{-1} x$ is a Lyapunov function for the model (2.1) on Ω.*

Proof We need to prove that the system has a Lyapunov function Q and that $Q' \leq 0$ on $\Omega \subset \mathbb{R}^{11}_+$. We have

$$(F-V)x = \begin{bmatrix} -aE+\beta_A A+\beta_P P+\beta_I I+\beta_N J_N+\beta_H J_H \\ \lambda_A E - bA \\ \lambda_P E - cP \\ \lambda_I E+\sigma_P P - dI \\ \rho_E E+\rho_A A+\rho_P P - eJ_N \\ \varepsilon_A A+\varepsilon_P P+\varepsilon_I I+\varepsilon_N J_N - fJ_H+\varepsilon_D J_I \\ \theta_A A+\theta_P P+\theta_I I+\theta_N J_N+\theta_H J_H - gJ_I \end{bmatrix}.$$

Evaluating $f(x,y) = (F-V)x - \mathcal{F}(x,y) + \mathcal{V}(x,y)$, as given in (4.5), yields

$$f(x,y) = \begin{bmatrix} (\beta_A A + \beta_P P + \beta_I I + \beta_N J_N + \beta_H J_H)\left(1 - \dfrac{S}{N - Q_S - Q_L - J_I}\right) \\ 0 \\ 0 \\ 0 \\ 0 \\ 0 \\ 0 \end{bmatrix}.$$

Now, one can show that $1 - \dfrac{S}{N - Q_S - Q_L - J_I} \geq 0$ as follows:

$$\begin{aligned} N &\geq Q_S + Q_L + J_I + S, \\ N - Q_S - Q_L - J_I &\geq S, \\ 1 &\geq \frac{S}{N - Q_S - Q_L - J_I}, \\ 1 - \frac{S}{N - Q_S - Q_L - J_I} &\geq 0. \end{aligned}$$

Therefore, $f(x,y) \geq 0$.

Differentiating the Lyapunov function gives

$$\begin{aligned} Q' &= w^T V^{-1} x'(t), \\ &= w^T V^{-1}(F - V)x - w^T V^{-1} f(x,y), \\ &= w^T (V^{-1}F)x - w^T (V^{-1}V)x - w^T V^{-1} f(x,y), \\ &= (R_c - 1) w^T x - w^T V^{-1} f(x,y), \\ &\leq 0 \text{ whenever } R_c \leq 1, \end{aligned}$$

since $w^T \geq 0$, $V^{-1} \geq 0$ and $f(x,y) \geq 0$. Hence Q is a Lyapunov function for the model (2.1) on $\Omega \subset \mathbb{R}^{11}_+$; thus, the DFE is asymptotically stable.

Furthermore, $Q' = 0$ only at the DFE (E_0). Hence the largest invariant set contained in the set Ω is reduced to the DFE. Since we are in a compact positively invariant set, by the LaSalle's invariance principle [27], the DFE is globally asymptotically stable in Ω.

4.2. Existence of endemic equilibrium

In this section, we investigate the existence of an endemic equilibrium by putting the right-hand side of the system (2.1) equal to zero and solving the equations simultaneously. We get

$$\begin{aligned} \hat{A} &= \frac{\lambda_A}{b}\hat{E}, \qquad \hat{P} = \frac{\lambda_P}{c}\hat{E}, \qquad \hat{I} = \frac{(c\lambda_I + \sigma_P \lambda_P)}{cd}\hat{E}, \\ \hat{Q_S} &= \frac{\rho_S}{\xi}\hat{S}, \qquad \hat{Q_L} = \frac{\alpha_L \xi + \alpha_S \rho_S}{h\xi}\hat{S}, \end{aligned}$$

$$\hat{J}_N = \frac{(\rho_E bc + \rho_A \lambda_A c + \rho_P \lambda_P b)}{bce}\hat{E},$$
$$\hat{J}_H = \frac{1}{f}\left[N_\varepsilon + \frac{\varepsilon_D (fM_\theta + \theta_H N_\varepsilon)}{m}\right]\hat{E},$$
$$\hat{J}_I = \frac{(fM_\theta + \theta_H N_\varepsilon)}{m}\hat{E},$$
$$\hat{R} = \frac{1}{\mu}\left[Z + \frac{\gamma_H}{f}N_\varepsilon + \left(\frac{\gamma_H \varepsilon_D}{f} + \gamma_D\right)\frac{(fM_\theta + \theta_H N_\varepsilon)}{m}\right]\hat{E},$$

where

$$Z = \frac{\gamma_A \lambda_A}{b} + \frac{\gamma_I (c\lambda_I + \sigma_P \lambda_P)}{cd} + \frac{\gamma_N (\rho_E bc + \rho_A \lambda_A c + \rho_P \lambda_P b)}{bce},$$
$$M_\theta = \left(\frac{\theta_A \lambda_A}{b} + \frac{\theta_P \lambda_P}{c} + \frac{\theta_I (c\lambda_I + \sigma_P \lambda_P)}{cd} + \frac{\theta_N (\rho_E bc + \rho_A \lambda_A c + \rho_P \lambda_P b)}{bce}\right),$$
$$N_\varepsilon = \left(\frac{\varepsilon_A \lambda_A}{b} + \frac{\varepsilon_P \lambda_P}{c} + \frac{\varepsilon_I (c\lambda_I + \sigma_P \lambda_P)}{cd} + \frac{\varepsilon_N (\rho_E bc + \rho_A \lambda_A c + \rho_P \lambda_P b)}{bce}\right)$$

Note that $N'(t) = \Lambda - \delta_H J_H(t) - \delta_D J_I(t) - \mu N(t)$. Therefore, the equilibrium state $N'(t) = 0$ implies that $\hat{N}(t) = \frac{1}{\mu}\left(\Lambda - \delta_H \hat{J}_H(t) - \delta_D \hat{J}_I(t)\right)$.

To find a relation between $\hat{S}$ and $\hat{E}$, the first two equations of the model can be written as follows:

$$\Lambda - \frac{aR_c\mu}{\Lambda - \frac{T}{m}\hat{E} - \mu a_2 \hat{S}}\hat{E}\hat{S} = a_1 \hat{S}, \tag{4.6}$$

$$\frac{aR_c\mu}{\Lambda - \frac{T}{m}\hat{E} - \mu a_2 \hat{S}}\hat{E}\hat{S} = a\hat{E}, \tag{4.7}$$

where

$$a_1 = \frac{\eta\xi h - h\lambda_S \rho_S - \lambda_L (\alpha_L \xi + \alpha_S \rho_S)}{\xi h}, \qquad a_2 = \left(\frac{\rho_S}{\xi} + \frac{(\alpha_L \xi + \alpha_S \rho_S)}{\xi h}\right),$$

$$T = M_\theta c_M + N_\varepsilon c_N,$$

$$c_M = \delta_H \varepsilon_D + f(\mu + \delta_D), \qquad c_N = \delta_H g + \theta_H (\mu + \delta_D).$$

Solving Eq (4.6) for $\hat{E}$ gives

$$\hat{E} = \frac{\left(\Lambda - a_1 \hat{S}\right)\left(\Lambda - \mu a_2 \hat{S}\right)}{\left(\Lambda - a_1 \hat{S}\right)\frac{T}{m} + aR_c\mu\hat{S}}. \tag{4.8}$$

Solving Eq (4.7) also for $\hat{E}$ gives

$$\hat{E} = \frac{\left[\Lambda - \mu\,(R_c + a_2)\,\hat{S}\right] m}{T}. \tag{4.9}$$

Solving Eqs (4.8) and (4.9) together gives

$$\hat{S} = \frac{\Lambda\,(T - a\,m)}{a_1\,T - a\,\mu\,m(R_c + a_2)}. \tag{4.10}$$

Substituting the expression of $\hat{S}$ from (4.10) into (4.9) gives

$$\hat{E} = \frac{m\,\Lambda\left[\mu\,(R_c + a_2) - a_1\right]}{a\,m\,\mu\,(R_c + a_2) - a_1\,T}. \tag{4.11}$$

Note that $a_1 = \mu\,(a_2 + 1)$; therefore, $\hat{S}$ and $\hat{E}$ can be written in the form

$$\hat{S} = \frac{(\Lambda/\mu)\,(a\,m - T)}{a\,m(R_c + a_2) - (a_2 + 1)\;T} \tag{4.12}$$

$$\hat{E} = \frac{m\,\Lambda\,(R_c - 1)}{a\,m\,(R_c + a_2) - (a_2 + 1)\,T}. \tag{4.13}$$

Note that the expressions a, m, a_2 and T are positive. One can also show that $(a\,m - T)$ is positive. Now, we check the signs of both $\hat{E}$ and $\hat{S}$ for the following cases:

(I) $R_c > 1$**:** the denominators of $\hat{E}$ and $\hat{S}$ can be shown to be positive as follows:

$$a\,m\,(R_c + a_2) - (a_2 + 1)\,T > a\,m\,(1 + a_2) - (a_2 + 1)\,T = (1 + a_2)\,(a\,m - T) > 0.$$

Clearly, both of the expressions of $\hat{E}$ and $\hat{S}$ are positive, resulting in an endemic equilibrium $E_e = \left(\hat{S}, \hat{E}, \hat{A}, \hat{P}, \hat{I}, \hat{Q}_S, \hat{Q}_L, \hat{J}_N, \hat{J}_H, \hat{J}_I, \hat{R}\right)$.

(II) $R_c = 1$**:** one can easily verify that the expressions (4.12) and (4.13) are reduced to the DFE (E_0) since $a\,m\,(R_c + a_2) - (a_2 + 1)\,T > 0$.

(III) $R_c < 1$**:** $\hat{S}$ and $\hat{E}$ are always of different signs as it is clear from the expressions (4.12) and (4.13). Therefore, there is no endemic equilibrium.

4.3. Bifurcation analysis

This section uses the center manifold theorem, as described in [28], to check if any type of bifurcation exists.

To apply the theorem, we rewrite the system (2.1) in the following formulation:

$$\frac{dx_1}{dt} = \Lambda - \frac{(\beta_A x_3 + \beta_P x_4 + \phi x_5 + \beta_N x_8 + \beta_H x_9)\,x_1}{N - x_6 - x_7 - x_{10}} - \eta\,x_1 + \lambda_S\,x_6 + \lambda_L x_7$$

$$
\begin{aligned}
\frac{dx_2}{dt} &= \frac{(\beta_A x_3 + \beta_P x_4 + \beta_I x_5 + \beta_N x_8 + \beta_H x_9)\, x_1}{N - x_6 - x_7 - x_{10}} - a\, x_2 \\
\frac{dx_3}{dt} &= \lambda_A x_2 - b\, x_3 \\
\frac{dx_4}{dt} &= \lambda_P x_2 - c\, x_4 \\
\frac{dx_5}{dt} &= \lambda_I\, x_2 + \sigma_P\, x_4 - d\, x_5 \\
\frac{dx_6}{dt} &= \rho_S\, x_1 - \xi\, x_6 \\
\frac{dx_7}{dt} &= \alpha_L\, x_1 + \alpha_S\, x_6 - h\, x_7 \\
\frac{dx_8}{dt} &= \rho_E\, x_2 + \rho_A\, x_3 + \rho_P\, x_4 - e\, x_8 \\
\frac{dx_9}{dt} &= {}_A\, x_3 + \varepsilon_P\, x_4 + \varepsilon_I\, x_5 + \varepsilon_N\, x_8 + \varepsilon_D\, x_{10} - f\, x_9 \\
\frac{dx_{10}}{dt} &= \theta_A\, x_3 + \theta_P\, x_4 + \theta_I\, x_5 + \theta_N\, x_8 + \theta_H\, x_9 - g\, x_{10} \\
\frac{dx_{11}}{dt} &= \gamma_A\, x_3 + \gamma_I\, x_5 + \gamma_N\, x_8 + \gamma_H\, x_9 + \gamma_D\, x_{10} - \mu\, x_{11}.
\end{aligned} \tag{4.14}
$$

Take $\beta_I = \phi$ to be the bifurcation parameter and $\beta_I^* = \phi^*$ to be the corresponding bifurcation value at $R_c = 1$. Then, R_c can be written as

$$R_c = \frac{\phi\,(c\lambda_I + \sigma_P\lambda_P)}{a\,c\,d} + K,$$

where $K = R_A + R_P + R_N + R_H$.

At $R_c = 1$, the bifurcation value is

$$\phi^* = \frac{a\,c\,d\,(1-K)}{(c\lambda_I + \sigma_P\lambda_P)}. \tag{4.15}$$

System (4.14) has the following Jacobian at the DFE E_0 and $\beta_I = \phi^*$:

$$J(E_0)|_{\phi^*} = \begin{bmatrix} -\eta & 0 & -\beta_A & -\beta_P & -\phi^* & \lambda_S & \lambda_L & -\beta_N & -\beta_H & 0 & 0 \\ 0 & -a & \beta_A & \beta_P & \phi^* & 0 & 0 & \beta_N & \beta_H & 0 & 0 \\ 0 & \lambda_A & -b & 0 & 0 & 0 & 0 & 0 & 0 & 0 & 0 \\ 0 & \lambda_P & 0 & -c & 0 & 0 & 0 & 0 & 0 & 0 & 0 \\ 0 & \lambda_I & 0 & \sigma_P & -d & 0 & 0 & 0 & 0 & 0 & 0 \\ \rho_S & 0 & 0 & 0 & 0 & -\xi & 0 & 0 & 0 & 0 & 0 \\ \alpha_L & 0 & 0 & 0 & 0 & \alpha_S & -h & 0 & 0 & 0 & 0 \\ 0 & \rho_E & \rho_A & \rho_P & 0 & 0 & 0 & -e & 0 & 0 & 0 \\ 0 & 0 & \varepsilon_A & \varepsilon_P & \varepsilon_I & 0 & 0 & \varepsilon_N & -f & \varepsilon_D & 0 \\ 0 & 0 & \theta_A & \theta_P & \theta_I & 0 & 0 & \theta_N & \theta_H & -g & 0 \\ 0 & 0 & \gamma_A & 0 & \gamma_I & 0 & 0 & \gamma_N & \gamma_H & \gamma_D & -\mu \end{bmatrix}$$

One can prove that the constant term of the characteristic equation of the above matrix is zero. Therefore, at least one of the eigenvalues is zero. The right and left eigenvectors (w and v, respectively) corresponding to the simple eigenvalue 0 are:

$w = [w_1 \quad w_2 \quad ... \quad w_{11}]^T$, and $v = [v_1 \quad v_2 \quad ... \quad v_{11}]^T$,

where,

$$w_1 = \frac{h\xi\, a}{h\rho_S\lambda_S + \lambda_L(\alpha_L\xi + \alpha_S\rho_S) - h\xi\,\eta},$$
$$w_2 = 1,$$
$$w_3 = \frac{\lambda_A}{b},$$
$$w_4 = \frac{\lambda_P}{c},$$
$$w_5 = \frac{c\lambda_I + \sigma_P\lambda_P}{dc},$$
$$w_6 = \frac{a\rho_S h}{h\rho_S\lambda_S + \lambda_L(\alpha_L\xi + \alpha_S\rho_S) - h\xi\,\eta},$$
$$w_7 = \frac{a(\alpha_L\xi + \alpha_S\rho_S)}{h\rho_S\lambda_S + \lambda_L(\alpha_L\xi + \alpha_S\rho_S) - h\xi\,\eta},$$

$$w_8 = \frac{\rho_E bc + \rho_A \lambda_A c + \rho_P \lambda_P b}{ecb},$$

$$w_9 = \frac{aR_H}{\beta_H},$$

$$w_{10} = \frac{1}{g}\left(\frac{\theta_A \lambda_A}{b} + \frac{\theta_P \lambda_P}{c} + \frac{\theta_I (c\lambda_I + \sigma_P \lambda_P)}{dc} + \frac{\theta_N (\rho_E bc + \rho_A \lambda_A c + \rho_P \lambda_P b)}{ecb} + \frac{\theta_H a R_H}{\beta_H}\right),$$

$$w_{11} = \frac{1}{\mu}\left(\frac{\gamma_A \lambda_A}{b} + \frac{\gamma_I (c\lambda_I + \sigma_P \lambda_P)}{dc} + \frac{\gamma_N (\rho_E bc + \rho_A \lambda_A c + \rho_P \lambda_P b)}{ecb} + \frac{\gamma_H a R_H}{\beta_H}\right)$$

$$+ \frac{\gamma_D}{\mu\, g}\left(\frac{\theta_A \lambda_A}{b} + \frac{\theta_P \lambda_P}{c} + \frac{\theta_I (c\lambda_I + \sigma_P \lambda_P)}{dc} + \frac{\theta_N (\rho_E bc + \rho_A \lambda_A c + \rho_P \lambda_P b)}{ecb} + \frac{\theta_H a R_H}{\beta_H}\right),$$

and

$$\begin{aligned}
v_1 &= 0,\\
v_2 &= \frac{m}{\beta_H g},\\
v_3 &= \frac{1}{b}\left[\frac{\beta_A m}{\beta_H g} + \frac{\rho_A}{e}\left(\frac{\beta_N m}{\beta_H g} + \varepsilon_N + \frac{\theta_N \varepsilon_D}{g}\right) + \varepsilon_A + \frac{\theta_A \varepsilon_D}{g}\right],\\
v_4 &= \frac{1}{c}\left[\frac{\beta_P m}{\beta_H g} + \frac{\sigma_P}{d}\left(\frac{\phi^* m}{\beta_H g} + \varepsilon_I + \frac{\theta_I \varepsilon_D}{g}\right) + \frac{\rho_P}{e}\left(\frac{\beta_N m}{\beta_H g} + \varepsilon_N + \frac{\theta_N \varepsilon_D}{g}\right) + \varepsilon_P + \frac{\theta_P \varepsilon_D}{g}\right],\\
w_5 &= \frac{1}{d}\left(\frac{\phi^* m}{\beta_H g} + \varepsilon_I + \frac{\theta_I \varepsilon_D}{g}\right),\\
v_6 &= 0,\\
v_7 &= 0,\\
v_8 &= \frac{1}{e}\left(\frac{\beta_N m}{\beta_H g} + \varepsilon_N + \frac{\theta_N \varepsilon_D}{g}\right),\\
v_9 &= 1,\\
v_{10} &= \frac{\varepsilon_D}{g},\\
v_{11} &= 0.
\end{aligned}$$

We compute the following second-order derivatives:

$$\frac{\partial^2 f_i}{\partial x_j \partial x_k} \text{ and } \frac{\partial^2 f_i}{\partial x_j \partial \phi},\ i, j, k = 1, 2, \cdots 11,$$

where $f_i, i = 1, 2, \cdots 9$ denotes the right-hand side of the equation number i of the system (4.15). Then, we have the following second-order derivatives:

$$\frac{\partial^2 f_1}{\partial x_2 \partial x_9} = \frac{\beta_H}{S^*}, \quad \frac{\partial^2 f_1}{\partial x_2 \partial x_8} = \frac{\beta_N}{S^*}, \quad \frac{\partial^2 f_1}{\partial x_2 \partial x_5} = \frac{\phi}{S^*}, \quad \frac{\partial^2 f_1}{\partial x_2 \partial x_4} = \frac{\beta_P}{S^*}, \quad \frac{\partial^2 f_1}{\partial x_2 \partial x_3} = \frac{\beta_A}{S^*},$$

$$\frac{\partial^2 f_1}{\partial x_3 \partial x_{11}} = \frac{\beta_A}{S^*}, \quad \frac{\partial^2 f_1}{\partial x_3 \partial x_9} = \frac{\beta_A + \beta_H}{S^*}, \quad \frac{\partial^2 f_1}{\partial x_3 \partial x_8} = \frac{\beta_A + \beta_N}{S^*},$$

$$\frac{\partial^2 f_1}{\partial x_3 \partial x_5} = \frac{\beta_A + \phi}{S^*}, \quad \frac{\partial^2 f_1}{\partial x_3 \partial x_4} = \frac{\beta_A + \beta_P}{S^*}, \quad \frac{d^2 f_1}{dx_3{}^2} = \frac{2\beta_A}{S^*},$$

$$\frac{\partial^2 f_1}{\partial x_4 \partial x_{11}} = \frac{\beta_P}{S^*}, \quad \frac{\partial^2 f_1}{\partial x_4 \partial x_9} = \frac{\beta_P + \beta_H}{S^*}, \quad \frac{\partial^2 f_1}{\partial x_4 \partial x_8} = \frac{\beta_P + \beta_N}{S^*},$$

$$\frac{\partial^2 f_1}{\partial x_4 \partial x_5} = \frac{\beta_P + \phi}{S^*}, \quad \frac{d^2 f_1}{dx_4{}^2} = \frac{2\beta_P}{S^*},$$

$$\frac{\partial^2 f_1}{\partial x_5 \partial x_{11}} = \frac{\phi}{S^*}, \quad \frac{\partial^2 f_1}{\partial x_5 \partial x_9} = \frac{\phi + \beta_H}{S^*}, \quad \frac{\partial^2 f_1}{\partial x_5 \partial x_8} = \frac{\phi + \beta_N}{S^*},$$

$$\frac{d^2 f_1}{dx_5{}^2} = \frac{2\phi}{S^*},$$

$$\frac{\partial^2 f_1}{\partial x_8 \partial x_{11}} = \frac{\beta_N}{S^*}, \quad \frac{\partial^2 f_1}{\partial x_8 \partial x_9} = \frac{\beta_N + \beta_H}{S^*}, \quad \frac{d^2 f_1}{dx_8{}^2} = \frac{2\beta_N}{S^*},$$

$$\frac{\partial^2 f_1}{\partial x_9 \partial x_{11}} = \frac{\beta_H}{S^*}, \quad \frac{d^2 f_1}{dx_9{}^2} = \frac{2\beta_H}{S^*},$$

$$\frac{\partial^2 f_2}{\partial x_2 \partial x_9} = \frac{-\beta_H}{S^*}, \quad \frac{\partial^2 f_2}{\partial x_2 \partial x_8} = \frac{-\beta_N}{S^*}, \quad \frac{\partial^2 f_2}{\partial x_2 \partial x_5} = \frac{-\phi}{S^*}, \quad \frac{\partial^2 f_2}{\partial x_2 \partial x_4} = \frac{-\beta_P}{S^*},$$

$$\frac{\partial^2 f_2}{\partial x_2 \partial x_3} = \frac{-\beta_A}{S^*},$$

$$\frac{\partial^2 f_2}{\partial x_3 \partial x_{11}} = \frac{-\beta_A}{S^*}, \quad \frac{\partial^2 f_2}{\partial x_3 \partial x_9} = \frac{-\beta_A - \beta_H}{S^*}, \quad \frac{\partial^2 f_2}{\partial x_3 \partial x_8} = \frac{-\beta_A - \beta_N}{S^*},$$

$$\frac{\partial^2 f_2}{\partial x_3 \partial x_5} = \frac{-\beta_A - \phi}{S^*}, \quad \frac{\partial^2 f_2}{\partial x_3 \partial x_4} = \frac{-\beta_A - \beta_P}{S^*}, \quad \frac{d^2 f_2}{dx_3{}^2} = \frac{-2\beta_A}{S^*},$$

$$\frac{\partial^2 f_2}{\partial x_4 \partial x_{11}} = \frac{-\beta_P}{S^*}, \quad \frac{\partial^2 f_2}{\partial x_4 \partial x_9} = \frac{-\beta_P - \beta_H}{S^*}, \quad \frac{\partial^2 f_2}{\partial x_4 \partial x_8} = \frac{-\beta_P - \beta_N}{S^*},$$

$$\frac{\partial^2 f_2}{\partial x_4 \partial x_5} = \frac{-\beta_P - \phi}{S^*}, \quad \frac{d^2 f_2}{dx_4{}^2} = \frac{-2\beta_P}{S^*},$$

$$\frac{\partial^2 f_2}{\partial x_5 \partial x_{11}} = \frac{-\phi}{S^*}, \quad \frac{\partial^2 f_2}{\partial x_5 \partial x_9} = \frac{-\phi - \beta_H}{S^*}, \quad \frac{\partial^2 f_2}{\partial x_5 \partial x_8} = \frac{-\phi - \beta_N}{S^*},$$

$$\frac{d^2 f_2}{dx_5{}^2} = \frac{-2\phi}{S^*},$$

$$\frac{\partial^2 f_2}{\partial x_8 \partial x_{11}} = \frac{-\beta_N}{S^*}, \quad \frac{\partial^2 f_2}{\partial x_8 \partial x_9} = \frac{-\beta_N - \beta_H}{S^*}, \quad \frac{d^2 f_2}{dx_8{}^2} = \frac{-2\beta_N}{S^*},$$

$$\frac{\partial^2 f_2}{\partial x_9 \partial x_{11}} = \frac{-\beta_H}{S^*}, \quad \frac{d^2 f_2}{dx_9{}^2} = \frac{-2\beta_H}{S^*},$$

$$\frac{\partial^2 f_I}{\partial x_5 \partial \phi} = -1, \qquad \frac{\partial^2 f_2}{\partial x_5 \partial \phi} = 1.$$

The rest of the second-order derivatives are all zero.

Calculating the coefficients $\widetilde{a}$ and $\widetilde{b}$ as defined in Theorem 4.1 [28] by Castillo Chavez and Song gives

$$\begin{aligned}
\widetilde{a} &= \sum_{k,i,j=1}^{n} v_k\, w_i\, w_j \frac{\partial^2 f_k}{\partial x_i \partial x_j}(\phi^*, E_0) \\
&= -\frac{v_2 w_2}{S^*}(\beta_H w_9 + \beta_N w_8 + \phi w_5 + \beta_P w_4 + \beta_A w_3) \\
&\quad - \frac{v_2 w_3}{S^*}\left[\beta_A w_{11} + (\beta_A + \beta_H) w_9 + (\beta_A + \beta_N) w_8 + (\beta_A + \phi) w_5 + (\beta_A + \beta_P) w_4 + 2\beta_A w_3\right] \\
&\quad - \frac{v_2 w_4}{S^*}\left[\beta_P w_{11} + (\beta_P + \beta_H) w_9 + (\beta_P + \beta_N) w_8 + (\beta_P + \phi) w_5 + 2\beta_P w_4\right] \\
&\quad - \frac{v_2 w_5}{S^*}\left[\phi w_{11} + (\phi + \beta_H) w_9 + (\phi + \beta_N) w_8 + 2\phi w_5\right] \\
&\quad - \frac{v_2 w_8}{S^*}\left[\beta_N w_{11} + (\beta_N + \beta_H) w_9 + 2\beta_N w_8\right] - \frac{v_2 w_9 \beta_H}{S^*}(w_{11} + 2w_9).
\end{aligned}$$

$$\begin{aligned}
\widetilde{b} &= \sum_{k,i=1}^{n} v_k\, w_i \frac{\partial^2 f_k}{\partial x_i \partial \phi}(\phi^*, E_0) \\
&= v_1 w_5 \frac{\partial^2 f_I}{\partial x_5 \partial \phi} + v_2 w_5 \frac{\partial^2 f_2}{\partial x_5 \partial \phi}, \\
&= \frac{m\ (c\lambda_I + \sigma_P)}{cd\,\beta_H g}.
\end{aligned}$$

Obviously, $\widetilde{a} < 0$ and $\widetilde{b} > 0$. Therefore, the system has a forward transcritical bifurcation.

Remark: Since the system has a forward transcritical bifurcation, the endemic equilibrium is locally stable when $R_c > 1$ and unstable when $R_c < 1$.

Numerical simulation of the model (2.1) using the fitted parameters also illustrated that the system undergoes transcritical bifurcation. The MatCont package [29] was used to study the model's behaviour using the transmission rate from symptomatic individuals β_I as the bifurcation parameter. Figure 3 shows how the stability of the equilibrium state changes as β_I varies. It is clear that before the bifurcation point (where $\beta_I^* \approx 0.287$ and $R_c = 1$), the DFE is stable, and then the stability state

bifurcates to the endemic equilibrium branch after the bifurcation parameter passes the bifurcation point β_I^*. This indicates that for a high transmission rate $\beta_I > \beta_I^*$, the disease will persists in the population.

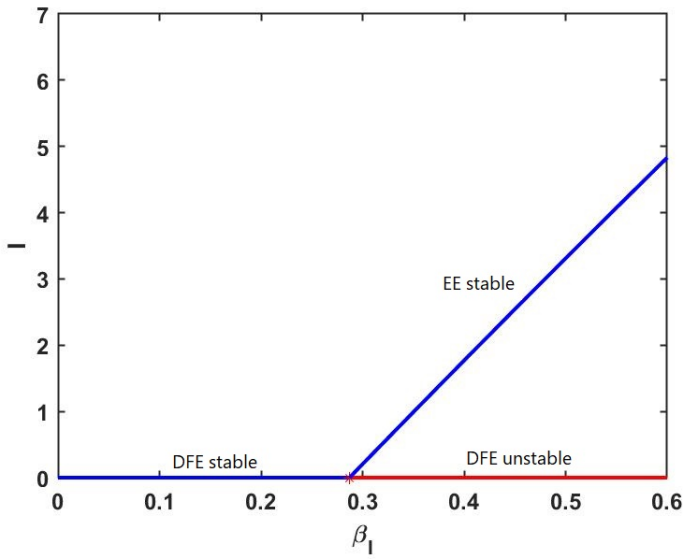

Figure 3. Bifurcation diagram of the system (2.1). The blue lines represent the stable states of the equilibrium points (DFE and endemic equilibrium (EE)), whereas the red line represents the unstable state of the equilibrium point (DFE). β_I is taken to be the bifurcation parameter, and the rest of the parameters were fixed at their estimated values as given in Table 3. At $\beta_I^* \approx 0.28707$, the system's stability switches from the DFE to the EE.

It is worth noticing that the expression derived for the bifurcation point in (4.15) matches exactly with its numerical value ($\beta_I^* \approx 0.28707$) when calculated using the fixed and fitted parameters.

5. Fitting of model parameters and numerical results

5.1. Fitting of model parameters

The proposed model (2.1) incorporates 36 parameters; some of them are available in literature and the remaining will be estimated using the daily reported cases for Oman. Data were collected for the period from August 4, 2020, to October 31, 2020 [30]. This period of time has been chosen for fitting because no vaccine was introduced at that time, so the effects of quarantine and isolation, in Oman, are better investigated. We employed the non-linear least square curve fitting approach [31] to fit the model to cumulative cases of the 89 days by using the Matlab optimization function fminsearchbnd. To improve the fitting and get the best of it, we set the initial guess as found in the literature for those parameters that are already available in references, as shown in Table 3. We also set lower and upper bounds for each parameter depending on the estimation of some biological and precautionary measures criteria. The fixed parameters shown in Table 3 are based on Oman population statistics and a previous study [10] about COVID-19 in Oman. The remaining 24 parameters were fitted and are

listed in Table 3. The best fit curve of the model to the reported data is shown in Figure 4.

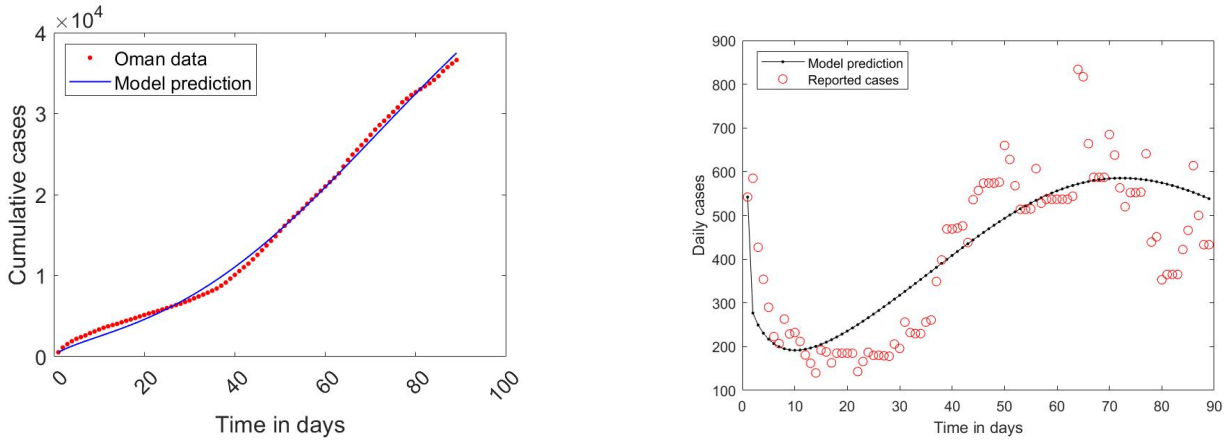

(a) Cumulative cases (b) Daily cases

Figure 4. Model fitting using cumulative cases in Oman from August 4 to October 31, 2020. (a) Model's fitted cumulative cases (blue line) vs confirmed cumulative cases (red circles). (b) Model's daily prediction (black dotted line) vs confirmed daily cases (red circles).

The graphs in Figure 5 represent the predicted situation of the pandemic for months following the three months used to estimate the parameters. Figure 5(a) shows a good prediction until the end of December 2020. However, the forecast is not fine when using more following months, as shown in Figure 5(b). This is because a new wave of the disease began at the end of December 2020.

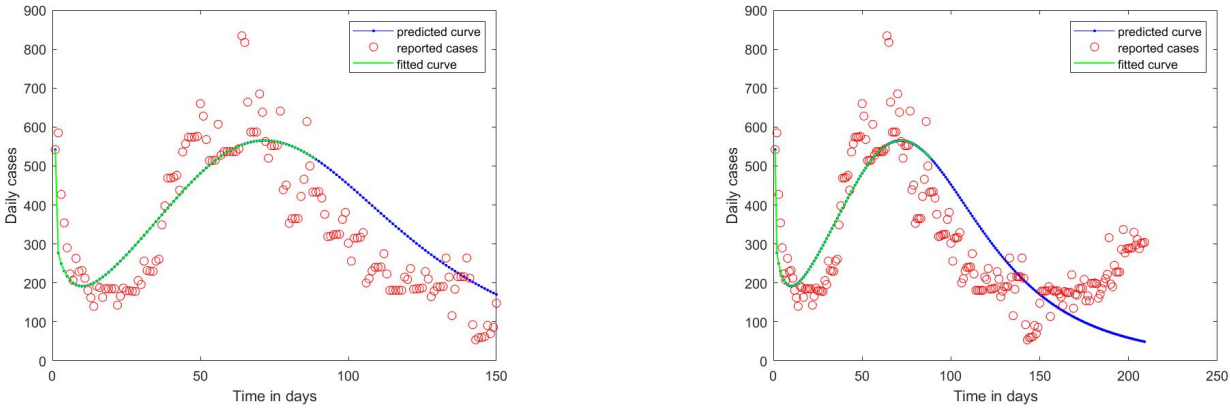

(a) Two months prediction (b) Four months prediction

Figure 5. Model prediction vs daily reported cases in Oman. The green dotted curves represent the period used in fitting (August 4 to October 31, 2020). The blue dotted curves represent the model prediction for the (a) two following months and the (b) four following months .

Table 3. Fitted values for the parameters in the model (2.1).

Parameter	Fitted value	initial guess reference	Parameter	Fitted value	initial guess reference
β_A	0.0015	[17]	ε_N	0.0869	[17]
β_P	0.7883	estimated	ε_D	0.1446	estimated
β_I	0.4269	[17]	α_L	0.2422	estimated
β_N	0.0032	[17]	α_S	0.0933	estimated
β_H	0.0027	[17]	ρ_S	0.4973	estimated
λ_S	0.4947	estimated	ρ_E	0.1995	[17]
λ_L	0.0167	estimated	ρ_A	0.3986	estimated
λ_P	0.3671	estimated	ρ_P	0.1918	estimated
λ_I	0.0933	[32]	θ_A	0.1549	estimated
ε_A	0.0154	estimated	θ_I	0.0157	[33]
ε_P	0.014	estimated	θ_N	0.0269	[17]
ε_I	0.2546	[33]	δ_H	0.0007	[34]
Parameter	fixed value	reference	Parameter	fixed value	reference
μ	0.0000334	$= 1/(82 * 365)$	γ_D	0.0155	[10]
$\Lambda = \mu N$	150	calculated	γ_H	0.028	[10]
λ_A	0.048	[10]	γ_N	0.081	[10]
σ_P	0.57	[10]	δ_D	0.00999	[10]
γ_A	0.043	[10]	θ_P	0.00842	[10]
γ_I	0.081	[10]	θ_H	0.0267	[10]

Using the fitted parameters, the approximate value of the reproduction number is $R_c \approx 1.202$ and the contribution from each transmission route is presented in the table below

Table 4. Transmission routes' contribution to R_c.

asymptomatic	presymptomatic	symptomatic	non-tested isolated	tested isolated
R_A	R_P	R_I	R_N	R_H
0.00017	0.52123	0.61809	0.00743	0.05553

The significant contribution to disease transmission comes from symptomatic and presymptomatic classes. These results agree with the findings in the review studies [35, 36] and the references therein.

5.2. Sensitivity analysis

This section is devoted to the use of sensitivity analysis to study the influence of different models' parameters on the spread of COVID-19. The sensitivity index ($\Upsilon_{\varphi}^{R_c}$) was measured when varying the reproduction number (R_c) with respect to the models' parameters by using the formula: $\Upsilon_{\varphi}^{R_c} = \dfrac{\partial R_c}{\partial \varphi}\dfrac{\varphi}{R_c}$.

The results are presented in Figure 6 and Table 5. Note that these results are based on using the set of estimated parameters in Table 3 as the baseline.

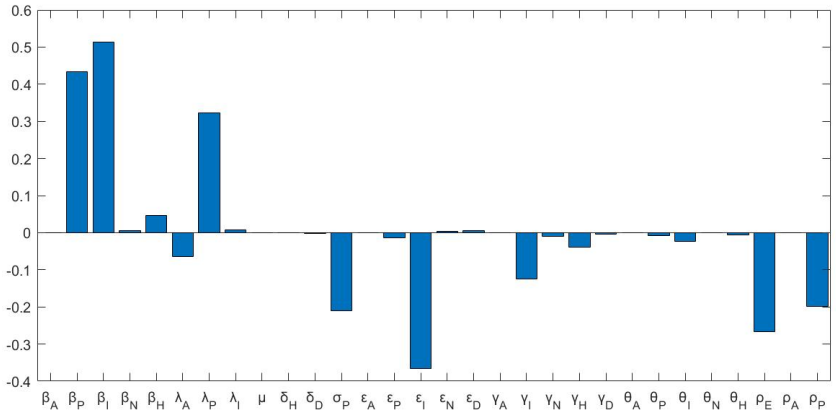

Figure 6. Sensitivity analysis chart of R_c to the estimated parameters. The closer the bar is to 1 (or –1), the more sensitive R_c is to an increase (or decrease) in the corresponding parameter.

Table 5. Sensitivity analysis of the model (2.1).

Parameter (φ)	$\Upsilon_{\varphi}^{R_c}$	Parameter (φ)	$\Upsilon_{\varphi}^{R_c}$	Parameter (φ)	$\Upsilon_{\varphi}^{R_c}$
β_A	0.00014	δ_D	–0.00225	γ_H	–0.03949
β_P	0.43347	σ_P	–0.21114	γ_D	–0.00349
β_I	0.51403	ε_A	0.00003	θ_A	0.0001
β_N	0.00618	ε_P	–0.01439	θ_P	–0.00871
β_H	0.04618	ε_I	–0.3665	θ_I	–0.02283
λ_A	–0.06424	ε_N	0.00329	θ_N	0.00037
λ_P	0.32307	ε_D	0.00575	θ_H	–0.00565
λ_I	0.00828	γ_A	–0.00025	ρ_E	–0.26707
μ	–0.00019	γ_I	–0.12464	ρ_A	–0.00001
δ_H	–0.00099	γ_N	–0.00984	ρ_P	–0.19920

It is clear that the transmission rate from symptomatic individuals (β_I) has the most impact on disease spreading, followed by the transmission rate from presymptomatic (β_P), then the rate at which exposed become presymptomatic (λ_P). Higher rates of λ_P indicate that it takes a shorter time for exposed ones to be infectious as preysmyptomatic, leading to higher transmission. On the other hand, the rate at which symptomatics are tested and moved to home isolation (ε_I) has the best influence on reducing the spread of disease, followed by the rate at which the exposed are home-isolated without testing (ρ_E) due to identification by contact tracing or behavioral self-isolation. In addition, the rate at which the presymptomatic class develops symptoms (σ_P) has a good influence on reducing the spread. The shorter it takes them to become symptomatic, the better it is to recognize them and control the spread. These findings can help policymakers in taking necessary action to prevent the disease from wide-spreading, keeping in mind the limitation of the study.

5.3. Numerical simulation

This section presents some numerical solutions for the model (2.1) based on the fitted parameters and ODE MATLAB solver *ode45*. The focus will be on the effects of different parameters on the model dynamics.

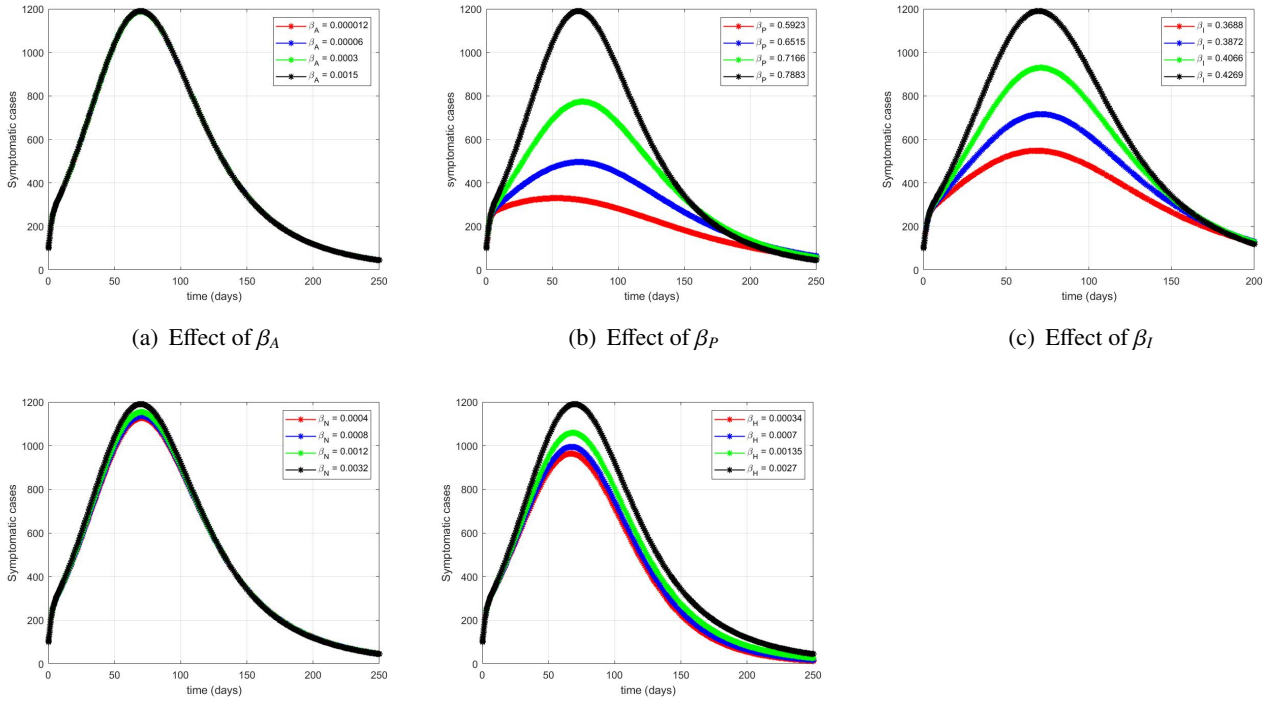

(a) Effect of β_A (b) Effect of β_P (c) Effect of β_I

(d) Effect of β_N (e) Effect of β_H

Figure 7. Effects of transmission rates from: (a) asymptomatic, (b) presymptomatic, (c) symptomatic, (d) non-tested home-isolated and (d) institutionally isolated individuals on disease dynamics.

In all graphs below, the black curve represents the fitted curve, while the others are used to illustrate the dynamics when a specific parameter is varied or controlled. The peaks of symptomatic and presymptomatic cases of the fitted curves are 1200 and 545 cases, respectively, in all graphs.

As shown in Figure 7, the transmission rates from presymptomatic (β_P) and symptomatic (β_I) classes have the most considerable impact on spreading the disease, while the transmission rates from asymptomatic (β_A) and non-tested home isolated (β_N) have the least impact. The transmission rate from the tested home isolated group (β_H) has a moderate effect.

To compare the strength of transmission from different groups, we take, for example, Figure 7(a),(b), which show the effects of the transmission rates from asymptomatic and presymptomatic, respectively. Increasing or decreasing the transmission rate from asymptomatic (β_A) by a factor of 5 has a negligible effect on the number of infected cases. On the other hand, increasing or decreasing the transmission rate from presymptomatic people (β_P) by a significantly smaller factor of 1.1 dramatically impacts the number of infected cases. This effect is clear from the curves in

Figure 7(b), where disease prevalence increases significantly with a slight increase in β_P. The behaviour mentioned above for β_P applies to the transmission rate from the symptomatic group (β_I) when it is varied by a factor of 1.05, as shown in Figure 7(c). Figure 7(d),(e) illustrates the dynamics when varying the transmission rates from non-tested and tested home isolated groups, respectively, by a factor of 2.

It is interesting to note that controlling the transmission rates from classes of strong influence can flatten the curve of infection, but the time it takes to reach the peak remains almost the same.

These simulations can hint at concentrating efforts to limit the disease spread by controlling the parameters of high impacts. In this current case, it is helpful to identify presymptomatic individuals by contact tracing and increasing testing intensity.

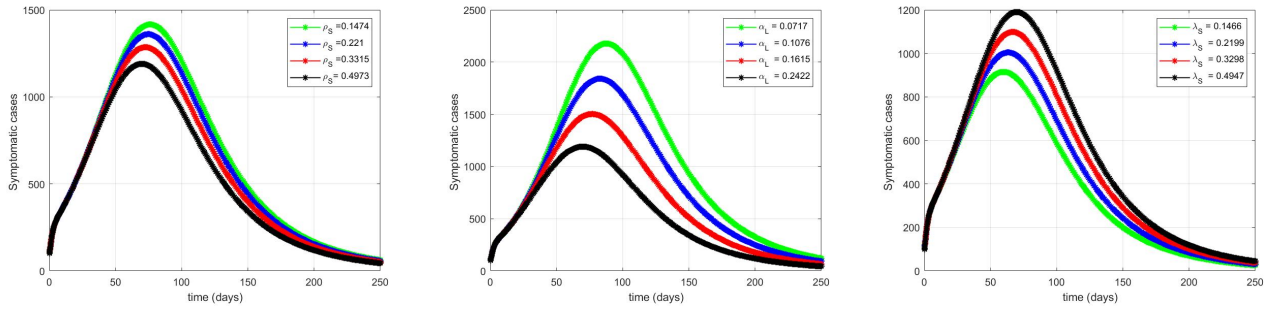

(a) Effect of ρ_S

(b) Effect of α_L

(c) Effect of λ_S

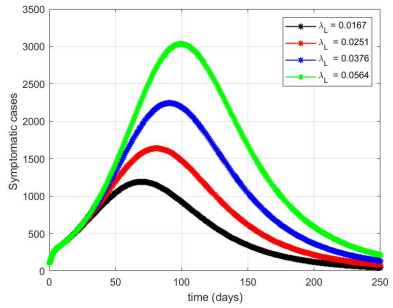

(d) Effect of λ_L

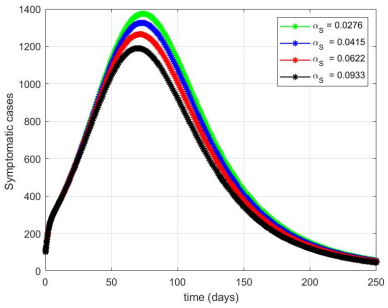

(e) Effect of α_S

Figure 8. Effects of short and long quarantine on the disease spread. Each graph represents the effects of: (a) short quarantine, (b) long quarantine, (c) leaving short quarantine, (d) leaving long quarantine and (e) moving from short to long quarantine.

Figure 8 shows the effects of short and long quarantines on disease dynamics. Although both types of quarantine have no direct influence on the reproductive number, they still considerably impact the disease transmission dynamics. As the more susceptible are quarantined for a short or long time (at rates ρ_S and α_L), the better it is for controlling the spread, and the peak of the infection curve will decrease. This behavior is clear from Figure 8(a) and (b). On the other hand, when more people leave their short or long quarantines (at rates λ_S and λ_L) return to the susceptible class, more infections occur, and the peak becomes higher, as shown in Figure 8(c) and (d). The current simulation shows that moving from short to long quarantine helps with reducing the infection when the rate of moving

(α_S) increases, as one can conclude from Figure 8(e).

The curves in all of the graphs are plotted when each parameter is changed by a factor of 1.5. Long quarantine has more influence on the spread of the disease, as it can be seen from Figure 8(b),(d).

Note that quarantine helps to lessen the number of infections and flatten the curve, though it speeds up the occurrence of the peak of infection.

The acts of instituting full or partial lockdown policies from time to time and putting a significant portion of communities under quarantine can mitigate disease spreading.

Figure 9 shows the effects of isolating symptomatic infectees institutionally or at home on disease spreading. It is clear from the graphs that increasing the isolation rates helps with reducing the intensity of infection and flattening the curve. From Figure 9(b), varying the rate of tested home isolation (ε_I) by a factor of 1.2 has a great influence on the disease the dynamics compared to dynamics resulting from varying the rate of institutional isolation (θ_I) by the same factor as shown in Figure 9(a).

Policymakers can utilize such observations, keeping in mind the limitation of the study, by enhancing home isolation over institutional isolation, where the latter is more costly and less effective. One may wonder how institutional isolation is less effective than home isolation, given that the first is more systematic and organized in a way that contact between isolated individuals is not likely to happen. The answer is that the number of isolations (whether at hospitals or other isolation centers) is limited and very small compared to the number at homes. Therefore, putting more effort into controlling and regulating home isolation is more economical and will help reduce infected cases.

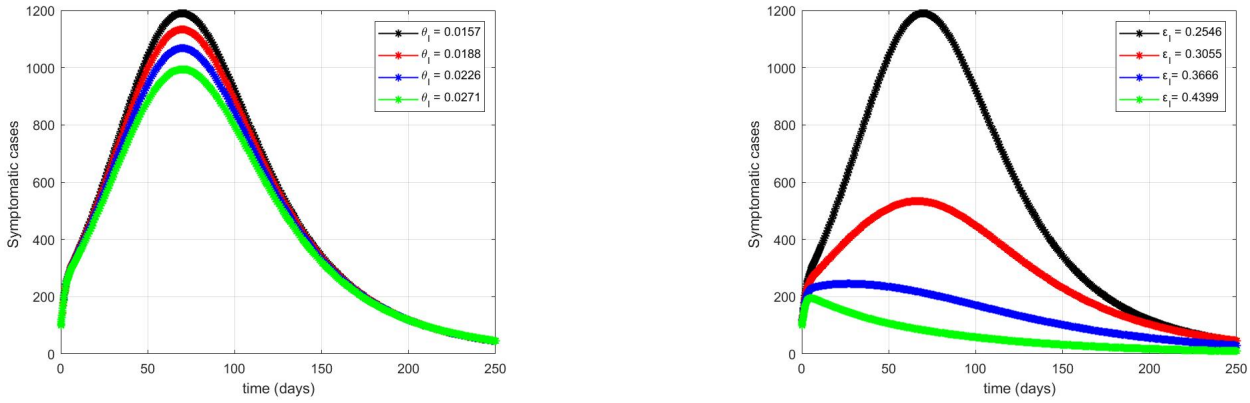

(a) Effect of θ_I (b) Effect of ε_I

Figure 9. Effects of isolating symptomatic individuals. Each graph shows the expected effects when testing symptomatic individuals and isolating them at (a) a health institution, or (b) at home.

Figure 10 illustrates the effects of isolating presymptomatic individuals on disease transmission dynamics. It can be concluded from the graphs that increasing the rates of isolation of presymptomatic individuals results in decreasing the overall infected cases. However, the presymptomatic group's challenge lies in the difficulty of identifying them, since they do not show any symptoms. Thus, increasing the intensity of random testing and contact tracing and promoting self-isolation are essential to control the spread from this group.

When comparing the three types of isolation, note that changing the rate of non-tested home

isolation (ρ_P) by a relatively small factor of 1.1, as shown in Figure 10(a), results in a considerable variations in the number of infections. On the other side, to get a comparable effect for the rates of institutional isolation (θ_P) and tested home isolation (ε_P), it is required to vary them by a higher factor of 2 as shown in Figure 10(b),(c). Hence, it is very crucial to deal with the presymptomatic group who are not identified through random testing. This mainly depends on human behaviour, so raising people's awareness on taking precautions and isolating themselves once there is a suspection of infection will definitely help containing the disease.

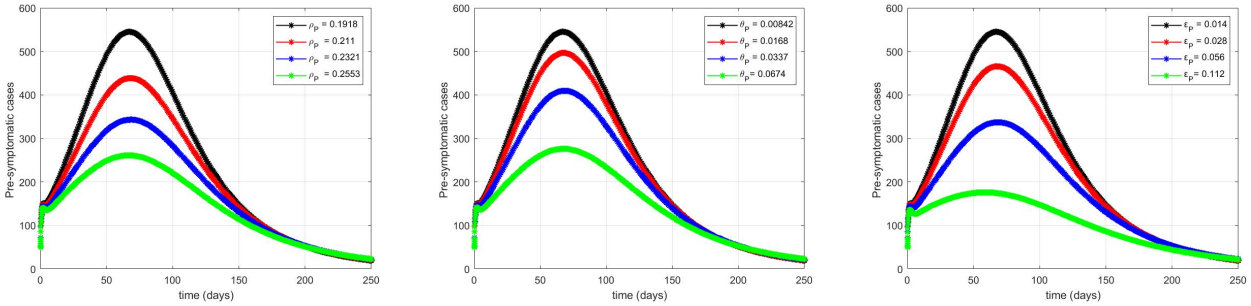

(a) Effect of ρ_P (b) Effect of θ_P (c) Effect of ε_P

Figure 10. Effects of isolating presymptomatic individuals on disease spread. Each graph displays the expected dynamics for isolating presymptomatic individuals (a) at home without testing, (b) at health institutions or (c) at home if tested positive.

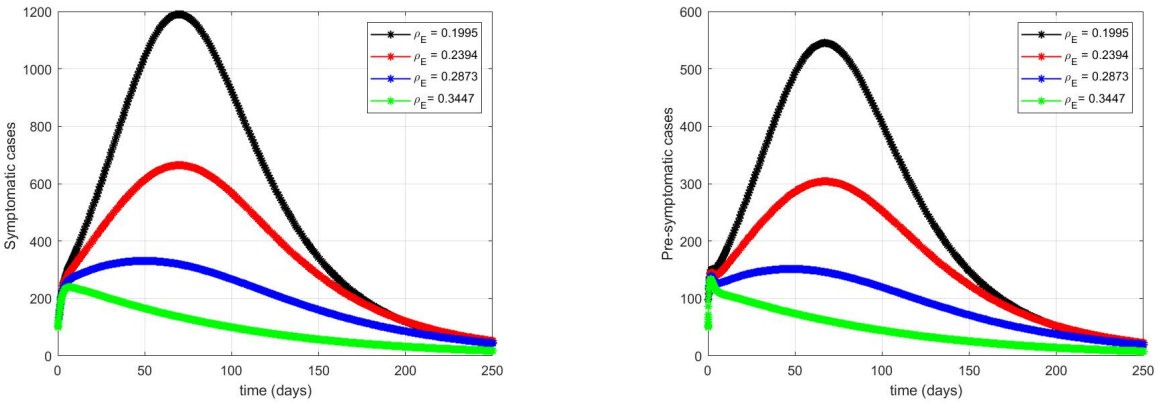

(a) Effect of ρ_E on symptomatic (b) Effect of ρ_E on presymptomatic

Figure 11. Effects of isolating exposed individuals on the disease spread. Each graph shows the expected effects when home-isolating exposed non-tested individuals on the number of (a) symptomatic and (b) presymptomatic infections.

Figure 11 demonstrates the effects of isolating exposed individuals at home without testing on the number of symptomatic (Figure 11(a)) and presymptomatic (Figure 11(b)) cases. The isolation of

exposed individuals could be due to contact tracing, travel regulations or a human behavior in response to awareness programs. The impact of varying the isolation rate ρ_E by a factor of 1.2 can be clearly seen in Figure 11, where the isolation rate is altered only by a factor of 1.2, but the variation in the maximum numbers of infections for both symptomatic and presymptomatic individuals is significant. Therefore, employing programs targeted to enhance human behavior toward dealing with the pandemic and utilizing technology for contact tracing will help control the fast spread of the disease.

6. Conclusions

A mathematical model for COVID-19 with different types of quarantine and isolation has been proposed, namely, short- and long-term quarantine, home isolation with or without testing and institutional isolation. The model has been fully analyzed to study the effects of the different types of quarantine and isolation on the disease transmission dynamics. The positivity and boundedness of solutions to the proposed model have been discussed. Model parameters were estimated by using the Oman dataset, and the best fit curve of the model to the reported data was illustrated graphically. The control reproduction number, R_c, was calculated using the NGM method and expressed as a sum of terms representing the contribution from all transmission routes. Using the obtained parameter values, the control reproduction number was estimated to be $R_c = 1.202$, with major contributions coming from symptomatic and presymptomatic transmissions. Sensitivity analysis for R_c (to model parameters) was carried out, and it was found that the symptomatic transmission rate, β_I, has the strongest positive impact on R_c, followed by the presymptomatic transmission rate, β_P. On the other hand, the home isolation rate for tested symptomatic individuals, ε_I, was found to have the strongest negative impact on R_c, followed by the home isolation rate for exposed individuals, ρ_E. The global asymptotic stability of the DFE was shown by using an appropriate Lyapunov function together with LaSalle's invariance principle whenever $R_c \leq 1$. The endemic equilibrium was found to exist if $R_c > 1$, and its local stability was deduced from the bifurcation analysis, since the system was found to have a forward transcritical bifurcation as a result of using the center manifold theorem and taking β_I to be the bifurcation parameter. The bifurcation results have been demonstrated graphically as well. Finally, the effects of some model parameters related to the different types of quarantine and isolation on the disease transmission dynamics were investigated numerically, and the results have been demonstrated graphically. The numerical results show that quarantine reduces the number of infected individuals and flattens the curve of infections, i.e., slowing the spread of the disease, with long quarantine having more impact on the disease transmission dynamics than short quarantine. Out of all of the different types of isolation, home isolation for tested symptomatic, non-tested exposed and non-tested presymptomatic individuals has the most significant impact on the disease transmission dynamics. These results agree very well with the obtained sensitivity results. Hence, adopting regulations for home quarantine and isolation and enhancing the culture of self-isolation through awareness programs are essential in controlling the spread of COVID-19.

This paper provides a deep insight into COVID-19 dynamics when many types of quarantine and isolations are employed. Vaccination can play an important role in controlling transmission and, accordingly, impacts the regulations of quarantine and isolation. However, it is not considered in this study. We will discuss this in future work.

Conflict of interest

The authors declare that there is no conflict of interest.

References

1. Q. Li, X. Guan, P. Wu, X. Wang, L. Zhou, Y. Tong, et al., Early transmission dynamics in Wuhan, China, of novel coronavirus–infected pneumonia, *N. Engl. J. Med.*, **382** (2020), 1199–1207. https://doi.org/ 10.1056/NEJMoa2001316
2. R. Dutta, L. Buragohain, P. Borah, Analysis of codon usage of severe acute respiratory syndrome corona virus 2 (SARS-CoV-2) and its adaptability in dog, *Virus Res.*, **288** (2020), 1–9. https://doi.org/10.1016/j.virusres.2020.198113
3. Y. C. Cao, Q. X. Deng, S. X. Dai, Remdesivir for severe acute respiratory syndrome coronavirus 2 causing COVID-19: An evaluation of the evidence, *Travel Med. Infect. Dis.*, **35** (2020), 1–6. https://doi.org/10.1016/j.tmaid.2020.101647
4. World Health Organization, *COVID 19 Public Health Emergency of International Concern (PHEIC). Global research and innovation forum: towards a research roadmap*, 2020.
5. *World Health Organization,* Coronavirus Disease (COVID-19), 2021. Available from: https://www.who.int/emergencies/diseases/novel-coronavirus-2019/situation-reports.
6. *Oman Observer*, Coronavirus, 2021. Available from: https://www.omanobserver.om/article/15089/ CORONAVIRUS/ hm-issues-orders-to-set-up-committee-on-COVID-19.
7. S. Kashte, A. Gulbake, S. F. El-Amin III, A. Gupta, COVID-19 vaccines: rapid development, implications, challenges and future prospects, *Human cell*, **34** (2021), 711–733. https://doi.org/10.1007/s13577-021-00512-4
8. M. S. Aronna, R. Guglielmi, L. M. Moschen, A model for COVID-19 with isolation, quarantine and testing as control measures, *Epidemics*, **34** (2021), 100437. https://doi.org/10.1016/j.epidem.2021.100437
9. A. Džiugys, M. Bieliūnas, G. Skarbalius, E. Misiulis, R. Navakas, Simplified model of COVID-19 epidemic prognosis under quarantine and estimation of quarantine effectiveness, *Chaos Solitons Fractals*, **140** (2020), 1–11. https://doi.org/10.1016/j.chaos.2020.110162
10. A. Varghese, S. Kolamban, V. Sherimon, E. M. Lacap, S. S. Ahmed, J. P. Sreedhar, et al., SEAMHCRD deterministic compartmental model based on clinical stages of infection for COVID-19 pandemic in Sultanate of Oman, *Sci. Rep.*, **11** (2021), 1–19. https://doi.org/10.1038/s41598-021-91114-5
11. N. Al-Salti, I. M. Elmojtaba, J. Mesquita, D. Pastore, M. Al-Yahyai Maryam. *Analysis of infectious disease problems (COVID-19) and their global impact*, Springer Nature, (2021), 219–244.
12. Z. Memon, S. Qureshi, B. R. Memon, Assessing the role of quarantine and isolation as control strategies for COVID-19 outbreak: a case study, *Chaos Solitons Fractals*, **144** (2021), 1–9. https://doi.org/10.1016/j.chaos.2021.110655
13. M. A. Khan, A. Atangana, E. Alzahrani, Fatmawati, The dynamics of COVID-19 with quarantined and isolation, *Adv. Differ. Equations*, **1** (2020), 1–22. https://doi.org/10.1186/s13662-020-02882-9

14. B. Tang, F. Xia, S. Tang, N. L. Bragazzi, Q. Li, X. Sun, et al., The effectiveness of quarantine and isolation determine the trend of the COVID-19 epidemics in the final phase of the current outbreak in China, *Int. J. Infect. Dis.*, **95** (2020), 288–293. https://doi.org/10.1016/j.ijid.2020.03.018

15. M. Ali, S. T. H. Shah, M. Imran, A. Khan, The role of asymptomatic class, quarantine and isolation in the transmission of COVID-19, *J. Biol. Dyn.*, **149** (2020), 389–408. https://doi.org/10.1080/17513758.2020.1773000

16. Y. Gu, S. Ullah, M. A. Khan, M. Y. Alshahrani, M. Abohassan, M. B. Riaz, Mathematical modeling and stability analysis of the COVID-19 with quarantine and isolation, *Results Phys.*, **34** (2022), 105284. https://doi.org/10.1016/j.rinp.2022.105284

17. S. S. Nadim, I. Ghosh, J. Chattopadhyay, Short-term predictions and prevention strategies for COVID-19: a model-based study, *Appl. Math. Comput.*, **404** (2021), 1–19. https://doi.org/10.1016/j.amc.2021.126251

18. C. N. Ngonghala, E. Iboi, S. Eikenberry, M. Scotch, C. R. MacIntyre, M. H. Bonds, et al., Mathematical assessment of the impact of non-pharmaceutical interventions on curtailing the 2019 novel Coronavirus, *Math. Biosci.*, **325** (2020), 108364. https://doi.org/10.1016/j.mbs.2020.108364

19. M. A. Oud, A. Ali, H. Alrabaiah, S. Ullah, M. A. Khan, S. Islam, A fractional order mathematical model for COVID-19 dynamics with quarantine, isolation, and environmental viral load, *Adv. Differ. Equations*, **2021** (2021), 1–19. https://doi.org/10.1186/s13662-021-03265-4

20. W. Ma, Y. Zhao, L. Guo, Y. Chen, Qualitative and quantitative analysis of the COVID-19 pandemic by a two-side fractional-order compartmental model, *ISA Trans.*, **124** (2022), 144–156. https://doi.org/10.1016/j.isatra.2022.01.008

21. N. Ma, W. Ma, Z. Li, Multi-Model selection and analysis for COVID-19, *Fractal Fractional*, **5** (2021), 1–12. https://doi.org/10.3390/fractalfract5030120

22. H. Mohammadi, S. Rezapour, A. Jajarmi, On the fractional SIRD mathematical model and control for the transmission of COVID-19: the first and the second waves of the disease in Iran and Japan, *ISA Trans.*, **124** (2022), 103–114. https://doi.org/10.1016/j.isatra.2021.04.012

23. D. Baleanu, M. H. Abadi, A. Jajarmi, K. Z. Vahid, J. J. Nieto, A new comparative study on the general fractional model of COVID-19 with isolation and quarantine effects, *Alexandria Eng. J.*, **61(6)** (2022), 4779–4791. https://doi.org/10.1016/j.aej.2021.10.030

24. M. R. Islam, A. Peace, D. Medina, T. Oraby, Integer versus fractional order SEIR deterministic and stochastic models of measles, *Int. J. Environ. Res. Public Health*, **17** (2020), 1–19. https://doi.org/10.3390/ijerph17062014

25. P. van den Driessche, J. Watmough, Reproduction numbers and sub-threshold endemic equilibria for compartmental models of disease transmission, *Mathematical biosciences*, **180(1-2)** (2002), 29–48. https://doi.org/10.1016/S0025-5564(02)00108-6

26. Z. Shuai, P. van den Driessche, Global stability of infectious disease models using Lyapunov functions, *SIAM J. Appl. Math.*, **73** (2013), 1513–1532. https://doi.org/10.1016/10.1137/120876642

27. J. P. LaSalle, *The Stability of Dynamical Systems*, Society for Industrial and Applied Mathematics, 1976.

28. C. Castillo-Chavez, B. Song, Dynamical models of tuberculosis and their applications, *Math. Biosci. Eng.*, **1** (2004), 361–404. https://doi.org/10.3934/mbe.2004.1.361

29. A. Dhooge, W. Govaerts, Y. A. Kuznetsov, H. G. E. Meijer, B. Sautois, New features of the software MatCont for bifurcation analysis of dynamical systems, *Math. Comput. Model. Dyn. Syst.*, **14** (2008), 147–175. https://doi.org/10.1080/13873950701742754

30. *Oman VS Covid*, The government official account for the efforts of countering COVID-19, 2021. Available from: https://twitter.com/OmanVSCovid19.

31. H. P. Gavin, The Levenberg-Marquardt algorithm for nonlinear least squares curve-fitting problems, *Mathematics*, **19** (2019), 1–19.

32. S. A. Lauer, Y. T. Grantz, Q. Bi, F. K. Jones, Q. Zheng, H. R. Meredith, et al., The incubation period of coronavirus disease 2019 (COVID-19) from publicly reported confirmed cases: estimation and application, *Ann. Intern. Med.*, **172** (2020), 577-582. https://doi.org/10.7326/M20-0504

33. J. Zhang, M. Litvinova, W. Wang, Y. Wang, X. Deng, X. Chen, et al., Evolving epidemiology and transmission dynamics of coronavirus disease 2019 outside Hubei province, China: A descriptive and modelling study, *Lancet Infect. Dis.*, **20** (2020), 793–802. https://doi.org/10.1016/S1473-3099(20)30230-9

34. S. Sanche, Y. T. Lin, C. Xu, E. Romero-Severson, N. Hengartner, R. Ke, High contagiousness and rapid spread of severe acute respiratory syndrome coronavirus 2, *Emerging Infect. Dis.*, **26** (2020), 1470–1477. https://doi.org/10.3201/eid2607.200282

35. M. Casey-Bryars,J. Griffin, C. McAloon, A. Byrne, J. Madden, D. Mc Evoy, et al., Presymptomatic transmission of SARS-CoV-2 infection: a secondary analysis using published data, *BMJ Open*, **11** (2021), e041240. http://dx.doi.org/10.1136/bmjopen-2020-041240

36. D. Buitrago-Garcia, D. Egli-Gany, M. J. Counotte, S. Hossmann, H. Imeri, A. M. Ipekci, et al., Occurrence and transmission potential of asymptomatic and presymptomatic SARS-CoV-2 infections: A living systematic review and meta-analysis, *PLoS Med.*, **17** (2020), e1003346. https://doi.org/10.1371/journal.pmed.1003346

AIMS Press